'See-through' deformation experiments on brittle–viscous norcamphor at controlled temperature, strain rate and applied confining pressure

P. Bauer, C. Rosenberg, M.R. Handy*

Institut für Geowissenschaften, Justus-Liebig-Universität Giessen, Giessen, Germany

Abstract

An integrated experimental–analytical deformational system allows the observation of evolving microstructures in rock analogues under an optical macroscope at controlled confining pressure ($P_c = 0.001$–0.3 MPa), temperature ($T = -10$–$150°C$) and strain rate (10^{-2}–10^{-6} s^{-1}). This system is ideally suited for studying grain-scale processes across the complete spectrum of deformational behaviour from brittle (cataclastic) to fully viscous (mylonitic) flow. The experimental system comprises two main elements: (1) a modified Urai–Means deformation rig, and (2) a steel pressure vessel that accommodates the deformation rig, yet is small enough to fit under an optical microscope. First results of controlled confining pressure experiments on fluid-bearing polycrystalline norcamphor, an organic quartz analogue, indicate that deformation involves a combination of dislocation creep and intergranular hydrofracturing leading to the formation of discrete shear surfaces comparable to C' planes in mylonite. At applied confining pressure, the relative activity of brittle and viscous deformation mechanisms varies across the sample. This in turn affects the distribution of strain on the sample scale. The pressure-dependence of strain localization in these experiments is interpreted to reflect a combination of local variations in the effective stresses and strain incompatibilities associated with the experimental, simple-shear configuration. © 2000 Elsevier Science Ltd. All rights reserved.

1. Introduction

The rheology of rocks and minerals depends both on their intrinsic properties (e.g. grain size, mineralogy) and on environmental variables (e.g. effective pressure, temperature and strain rate). The high temperatures and confining pressures of the crust and upper mantle are easily attained in some triaxial deformation machines (Tullis and Tullis, 1986), but the microstructures of the samples deformed in these machines cannot be viewed during deformation. Deformed samples are therefore quenched and slowly decompressed at the end of deformation in the expectation that their microstructure does not equilibrate with post-deformational conditions.

The difficulty of viewing microstructures during deformation has been partly overcome by shearing thin layers of rock-analogue materials directly under the optical polarizing macroscope (i.e. a low-power microscope) in so-called 'see-through' experiments (e.g. Means, 1989). When deformed at room temperature and pressure, these organic and inorganic materials develop microstructures that are similar, if not identical, to those found in real tectonites. Rock analogues simulate creep processes in rocks or minerals because their viscosities are very low (e.g. effective viscosity of norcamphor is 2.3 Pa s at $T = 28°C$, $\dot{\varepsilon} = 10^{-5}$ s^{-1}, data of Bons, 1993) despite the low temperatures and unnaturally high strain rates (10^{-2}–10^{-6} s^{-1}) necessary to perform the experiment within a reasonable time (hours to days). A list of rock analogues and their properties is available on request from the authors. A major shortcoming of see-through experiments so far is that they are not appropriate for studying dilational,

---

* Corresponding author.

E-mail address: mark.handy@geo.uni-giessen.de (M.R. Handy).
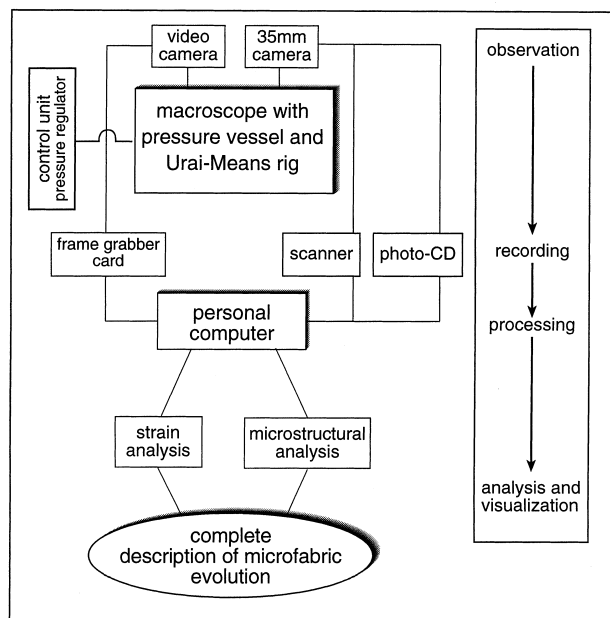
Fig. 1. Flow diagram of experimental–analytical system for see-through deformation experiments (see text).

pressure-dependent processes like cataclasis. This is because existing deformation machines, including the well-known Urai–Means shear rig (Means, 1989), are designed to vary temperature and strain rate, but not confining pressure.

In this paper, we present a new experimental system designed to facilitate the analysis of rock-analogue microstructures in see-through deformation experiments. This system incorporates technical innovations that enable rock analogues to be deformed to high shear strains at controlled confining pressure, temperature and strain rate. The first results of controlled pressure experiments on polycrystalline norcamphor that contain a pore fluid indicate that strain localization at the brittle–viscous transition is pressure-dependent. We discuss possible causes of this pressure-dependence and conclude by outlining further applications of this experimental system to the study of syn-tectonic, pressure- and temperature-sensitive geological processes.

2. Laboratory system for see-through experiments

The new laboratory system, depicted schematically in Fig. 1, allows the microfabric of a rock analogue material to be analyzed in transmitted light during deformation under applied confining pressure, controlled temperature and strain rate. In the following, we describe those components of the system that are new or have been extensively modified from existing machines. The heart of this system (Fig. 2a) comprises a low-power microscope with a long working-distance, zoom objective (generally referred to as a macroscope) and a pressure vessel containing a modified Urai–Means deformation rig.

2.1. The modified Urai–Means deformation rig

J. Urai designed and produced a see-through deformation rig (Urai, 1983) that is based in principle on an approach conceived by Mosher et al. (1975) and advanced by Means (1977, 1980, 1981) and Means and Xia (1981) to study the microstructural evolution of organic rock analogues in transmitted light. The Urai–Means deformation rig (Fig. 2b) comprises a synchronous motor connected through a flexible coupling to a spindle drive that moves a ram. In the deformation cell, this ram pushes one glass plate over another, thereby deforming the jacketed sample sandwiched in between. Light from the macroscope passes from bottom to top through windows in the deformation cell. The deformation cell contains a cooling/heating unit, a thermocouple and the sample holder (description in Herwegh and Handy, 1996). The organic rock analogue between the glass plates adheres to frosted grips whose orientation with respect to the ram's movement direction can be varied to simulate any strain configuration between the end-members simple shear (Fig. 2b) and plane strain, pure shear. The distance between these grips determines the shear zone width, and therefore also the strain rate at a constant motor-driven displacement rate. Friction along all other surfaces of the jacketed sample with the glass plates is minimized by coating the plates with silicon oil.

To conduct high strain experiments on brittle and brittle–viscous, as well as fully viscous materials, we modified the Urai–Means rig in three ways:

1. Installation of a new cooling unit comprising a refrigerator with a storage tank for the cooling liquid (kept at $-35°C$), a pump and a well-insulated tube connecting the deformation cell with the storage tank; isopropanol was found to be an efficient liquid coolant due to its low freezing temperature ($-70°C$). The control unit regulates both the heating/cooling elements (described below) and the rate of coolant flow, thereby ensuring exact control of the sample temperature.

2. Incorporation of Peltier semiconducting plates at the base of the deformation cell. These plates consist of two semiconducting materials that either heat or cool the sample in the deformation cell, depending on the polarity and voltage of the applied current. They ensure a more homogeneous temperature distribution within the deformation cell. They also alleviate thermal overstepping when heating the sample. Overstepping of up to $30°C$ was encoun-
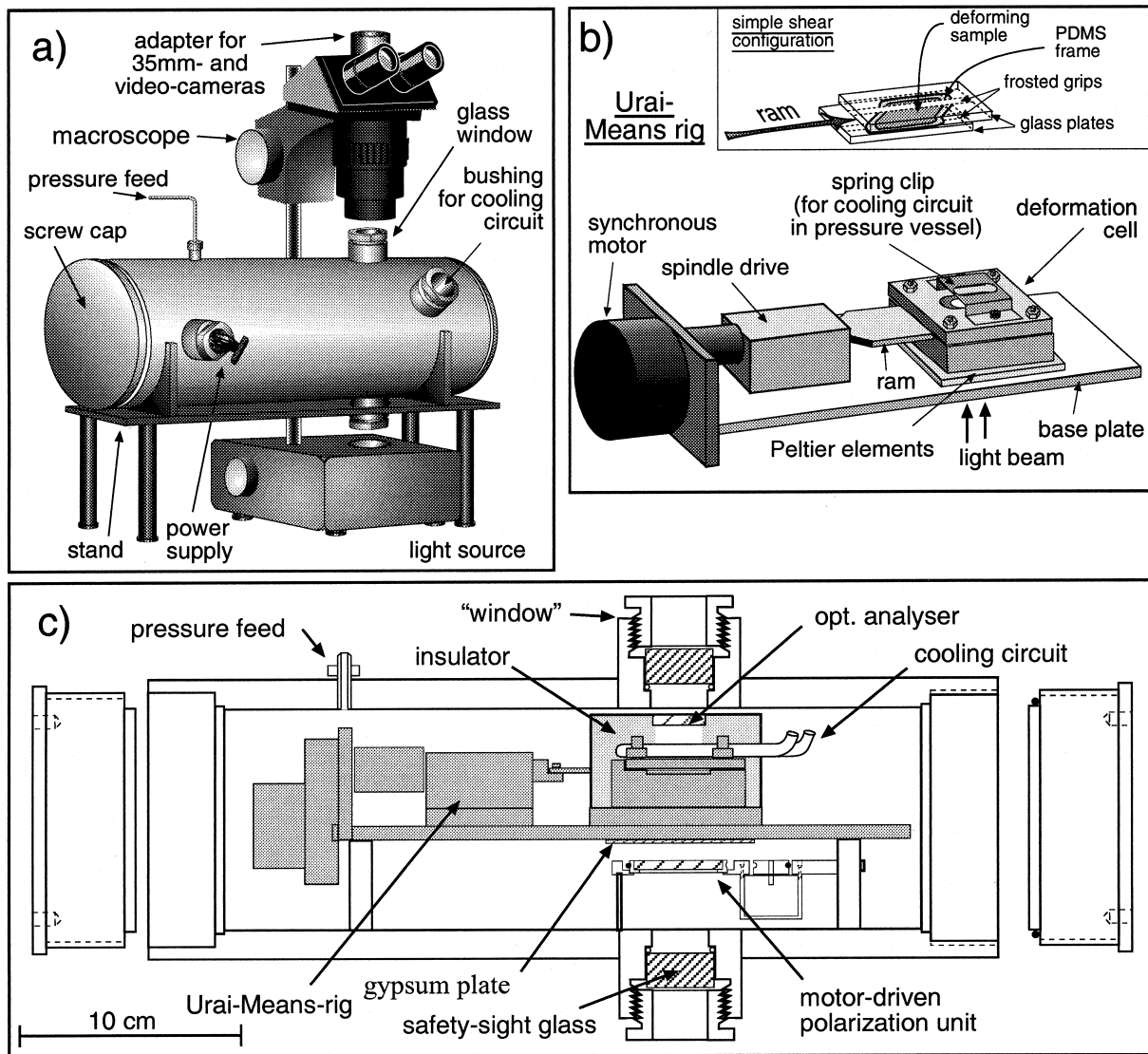
Fig. 2. Deformational and observational components of the experimental system used in this study: (a) macroscope with stage supporting the pressure vessel; (b) modified Urai–Means see-through deformation rig with inset above showing glass plates configured for simple shearing; (c) cutaway side view of the pressure vessel containing the deformation rig (see text for description).

tered during heating with the cylindrical heating elements in the original rig. Modifications (1) and (2) enable uniform heating or cooling of the sample over a different temperature range (−10–150°C) and with greater accuracy (±0.1°C) than with the unmodified rig (25–250°C, ±1°C). The lower temperature range allows one to deform a wider selection of commercially available rock analogues in deformation regimes from brittle (cataclastic) to fully viscous (mylonitic).

3. Lengthening the deformation cell in order to deform the sample to higher shear strains ($\gamma = 20$) than possible in the commercially available rig ($\gamma = 10$) at a given spacing (2 mm) of the frosted grips on the glass plates. Experience shows that in rock analogues deforming homogeneously by dislocation creep, microstructural steady state is only achieved at shear strains of $\gamma = 8$ (e.g. Herwegh and Handy, 1996). Even higher shear strains are necessary to attain microstructural steady state in materials undergoing heterogeneous deformation, such as at the brittle–viscous transition. As an aside, we note that not all experiments reported below used a lengthened deformation cell.

2.2. A pressure vessel for see-through deformation experiments

The pressure vessel accommodates the modified Urai–Means rig and fits on a stand under a Leica

M420 optical polarizing macroscope (Fig. 2a and c). The vessel is essentially a hollow cylinder (diameter 10 cm, length 38 cm, wall thickness 14 mm). This cylinder, as well as all system components subjected to applied pressure, is made entirely of stainless steel (SANDVIK 5R75, material number 1.4571). The openings at either end of the cylinder are sealed by screw caps with gasket rings. The vessel operates normally with gas or non-corrosive liquid confining media at pressures of up to 0.3 MPa and temperatures ranging from −10 to 150°C. The maximum test pressure of the vessel is 0.45 MPa. In the experiments reported below, the air pressure is adjusted manually with a manometer and two globe valves. If desired, pressure can also be varied with computer-controlled magnetic valves.

The pressure vessel has four cylinders protruding from its sides: the two front cylinders (Fig. 2a) accommodate pressure bushings for the cooling lines and power supplies of the deformation rig and polarization unit, whereas the other two cylinders at the top and bottom are equipped with glass windows to allow direct observation of the deforming sample in transmitted light under the macroscope. The glass in these windows is necessarily thick (15 mm) to withstand the maximum test pressure of 0.45 MPa. Because thick glass distorts polarized light, especially towards the edges of the windows, the polarization unit and λ-plate were installed inside the pressure vessel. A small, geared motor rotates the lower polarizer so that transmitted light observations with both crossed and parallel polarizers can be made without opening the vessel and interrupting the experiment.

The electrical seals are equipped with epoxy housing material and silicon-insulated cables. Twelve cables pass through the seal to power the motor, the Peltier elements, the thermocouple and the motor-driven polarization unit. The cooling circuit in the original Urai–Means rig cannot withstand the large pressure differences between the inside of the vessel and the externally supplied cooling liquid, so a conductive cooling loop comprising a steel tube (V4A) with thicker walls is clipped to the deformation cell. A metal plate mounted beneath the cooling loop enlarges the contact area with the deformation cell and ensures efficient cooling (Fig. 2c). The viewing windows in the deformation cell are insulated from the cooling unit with plastic inlays to avoid optical distortion associated with the large density fluctuations of air around the cooling unit in the vessel.

We point out that although the confining pressure within the pressure vessel can be varied, the pressure of any fluid or vapour trapped in the sealed sample between the glass plates in the deformation cell cannot be controlled or measured. This point is discussed further in the context of the experiments below.

3. Recording and analytical equipment

The microstructural evolution during an experiment is recorded continuously by a video camera connected to a personal computer (Fig. 1). The computer is equipped with a frame-grabber card to digitize the video signal at strain-rate dependent intervals (120 s in the experiment described below). The images are recorded and then processed with the public domain computer program, NIH-Image, to create time-lapse movies of the microstructural evolution. Black-and-white film with fine-grained emulsion is used for documenting the positions of tiny passive strain markers (in this case, corundum powder particles) strewn in the sample before deformation (Means, 1980). The choice of time interval depends on the rate of microstructural change, and hence on the strain rate as well as on the process being studied. During the experiments reported below, photographs were taken every hour, corresponding to a shear strain interval of $\gamma = 0.3$.

A characterization of the experimentally produced microstructure involves two analytical procedures, as shown schematically at the bottom of Fig. 1. Detailed microstructural analysis is carried out on the stored and previously processed images of the deforming sample. In the experiments below, this analysis included measuring the angle and length of shear surfaces, determining the orientation and size of grains and grain domains, and estimating the areal proportion of fluid in the sample. Strain analysis involves digitizing the positions of the passive marker particles on black-and-white photos with NIH-Image, and then using the program Marker Analysis (Bons et al., 1993) to calculate incremental strain grids from changes in the relative positions of these particles during the experiment. Strain is visualized as contour plots of axial ratios of the finite strain ellipse, as calculated at every node of the incremental strain grid.

4. Sample preparation and experimental conditions

To test the new deformational system, we deformed water-bearing ('wet') polycrystalline norcamphor ($C_7H_{10}O$) in simple shear at both atmospheric pressure (eight experiments) and at applied confining pressures, P_c, of 0.05–0.2 MPa (four experiments). All experiments were undrained (i.e. the water remained in the sample), and were conducted at a constant temperature (10°C) and shear strain rate (8×10^{-5} s^{-1}). Norcamphor has hexagonal crystallography, uniaxial negative optical properties (Bons, 1993), and has many crystallographic slip systems in common with quartz (Herwegh and Handy, 1996). Past studies have shown norcamphor to be an excellent analogue for naturally deformed metamorphic quartz (Herwegh et al., 1997).
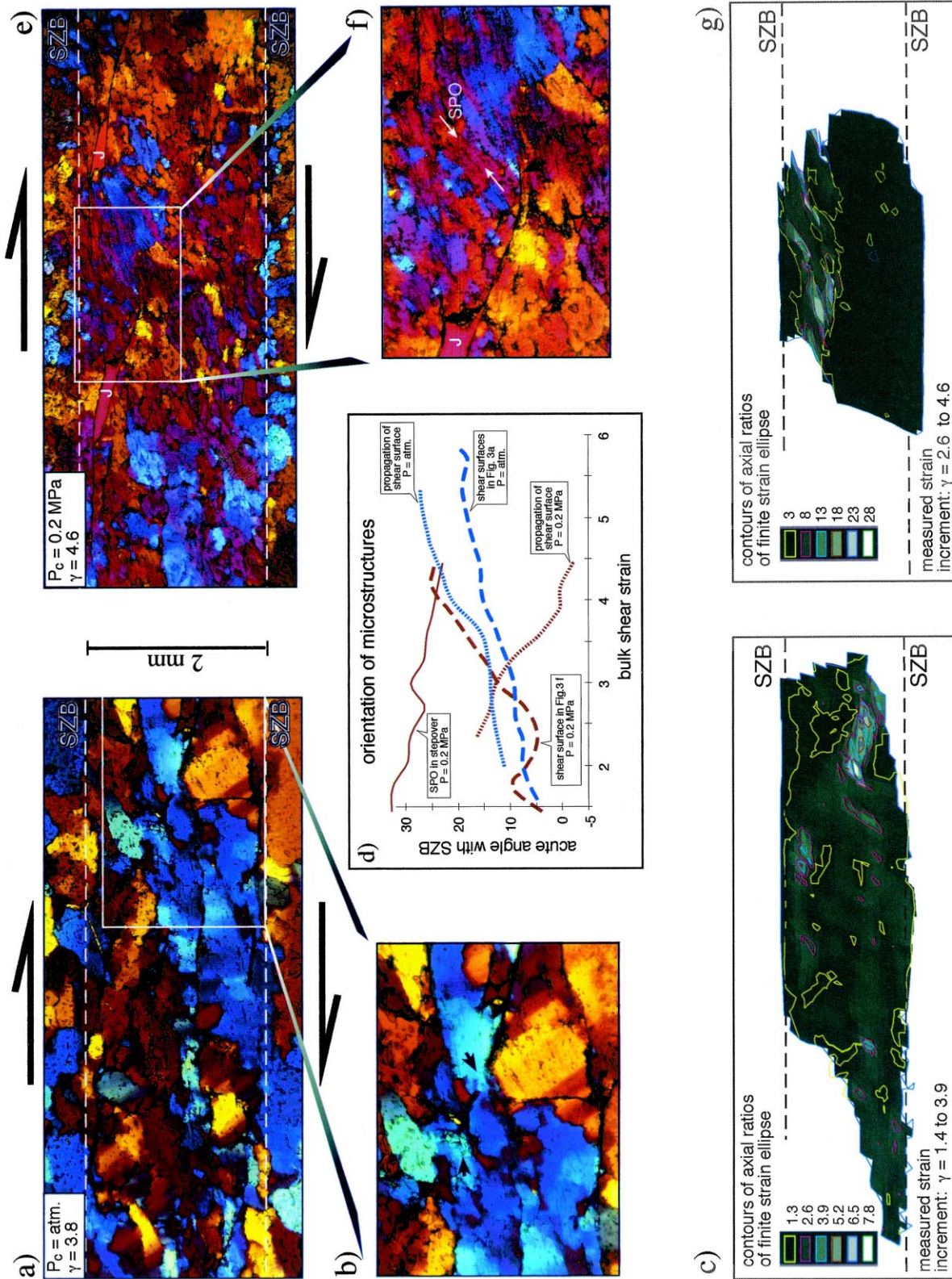
Fig. 3. Comparison of microstructures in simple shearing experiments at atmospheric pressure and at a confining pressure of 0.2 MPa: (a) Sheared sample at atmospheric pressure; (b) close-up of outlined area in (a). Black arrows point to tips of shear fractures; (c) contoured plot of incremental axial strain ratios of sample in (a), finite bulk strain is 2.5, measured at an interval of $\gamma = 0.5$, SZB is marked by dashed lines (compare with a); (d) change in orientation of microstructures with progressive shear; (e, f, and g) same as (a)–(c), but for sheared samples at applied confining pressure. Note extensional jogs marked J adjacent to the shear surfaces in (e) and (f). White arrows in (f) indicate average orientation of the grain shape preferred orientation (SPO) between overlapping shear surfaces. See text for explanation. Micrographs of samples viewed with crossed polarizers and inserted λ-plate. The temperature and shear strain rate in both types of experiments were $T = 10°C$ and $\dot{\gamma} = 8 \times 10^{-5} \ s^{-1}$.

Preparation of wet norcamphor samples is similar to that already described in Herwegh and Handy (1996) for dry (water-free) samples, so only deviations from this procedure that are pertinent to the wet experiments at applied confining pressure are described here. A cold-pressed wafer of norcamphor is encased in a thin frame of a polymer substance (polydimethylsiloxane, PDMS) between the glass slides. About 5–7 vol.% distilled water is added to create fluid pockets at grain boundaries and triple junctions. The PDMS frame is a viscous confining medium (Weijermars, 1986) and prevents leakage of water from the sample during the experiment. Therefore, the PDMS frame can be regarded as a jacket that also prevents the confining medium (in this case, compressed air) from penetrating the sample. After the wet norcamphor sample has been hot-pressed ($T = 45°C$) in the deformation cell for several days, the modified Urai–Means rig is placed in the pressure vessel and the sample is allowed to cool to the experimental temperature at atmospheric pressure. Throughout this procedure, we observed no change in the volume proportions of fluid and norcamphor in the samples. This, combined with the observed solubility of norcamphor in water (8 g/l water), indicates that the fluid pockets on grain boundaries and triple junctions are saturated with norcamphor. The fluid pockets do not appear to be interconnected, even though the dihedral angle between fluid and norcamphor is approximately $46°$, well below the critical value of $60°$ required for grain-edge fluid channels to form in an isotropic, crystalline aggregate (e.g. Holness, 1997). The lack of interconnection of the fluid pockets in our experiments, whether apparent or not, may be related to the fact that the average diameter of the norcamphor grains is much greater than the thickness of the sample between the glass plates.

Confining pressure is then increased slowly (= 0.07 MPa/h) to avoid the expulsion of fluid from grain-boundary inclusions. Upon attainment of the desired pressure, the deformation experiment can begin and the remaining procedure is the same as that without confining pressure. Provided that the pressure vessel is sealed carefully, experiments lasting longer than 50 h can be conducted without significant pressure loss. There was no evidence for any leakage of fluid or volume change of the sample. The average pore fluid pressure, P_f, is inferred to remain high (i.e. $P_f \leq P_c$) in the samples during the experiments reported below.

5. Pressure effects at the brittle to viscous transition

Fig. 3 shows the main microstructural differences between wet norcamphor deformed at atmospheric (Fig. 3a–c) and applied confining pressure (Fig. 3e–g). Irrespective of confining pressure, wet norcamphor deforms by a combination of dislocation creep (dynamic, grain-boundary migration recrystallization) and subordinate intergranular hydrofracturing. The intergranular fluid pockets serve as nucleation sites for fractures between dynamically recrystallizing grains. Depending on confining pressure, however, the relative activity of fracturing and dynamic recrystallization varies with location in the sample. This in turn affects the distribution of strain on the sample scale.

At atmospheric pressure, strain is distributed more evenly across the sample compared to the applied pressure experiments described below (Fig. 3c and g). Already at very low shear strains ($\gamma = 1$), extensional shear fractures nucleate at water-filled pockets along grain boundaries and then interconnect to form shear surfaces at low angles ($5–15°$) to the shear zone boundary, or SZB (see Means and Xia, 1981 for similar structures in deformed sodium nitrate). These shear surfaces are more or less evenly spaced within the shear zone (Fig. 3a). Their orientation with respect to the SZB is similar to that of synthetic C' surfaces in S–C mylonites (e.g. Platt and Vissers, 1980; Vauchez, 1987). The geometry of these shear surfaces and the absence of fractures in dry experiments at the same experimental conditions as above (Herwegh and Handy, 1996) are consistent with the idea that these surfaces originate as intergranular hydrofractures in the presence of pressurized fluid. Grain-boundary migration rates are also much lower than in dry experiments at comparable temperatures and strain rates, suggesting that fluid at the grain boundaries reduces grain-boundary mobility and therefore induces strain incompatibilities on the granular scale. With further strain, the shear surfaces rotate synthetically, while propagating at increasing angles to the SZB (Fig. 3d). The tips propagate sporadically by a combination of subcritical intergranular fracturing (arrows in Fig. 3b) and intracrystalline plasticity. Progressive shearing is associated with cataclastic grain-size reduction along the shear surfaces, concurrent with grain-size reduction by grain-boundary migration recrystallization in the rest of the sample. By finite shear strains of about $\gamma = 8$, the average grain size in the dynamically recrystallized parts of the sample has decreased from 350 μm to a steady-state value of 100 μm. Likewise, the length of shear surfaces per unit area of sample increases from 0.5 mm/mm^2 to a near steady-state value of 1.05 mm/mm^2.

In contrast, experiments at applied confining pressure reveal a striking asymmetry in both the strain distribution and in the length of shear surfaces on the sample scale. After only a few strain increments, shear surfaces nucleate as extensional shear fractures in the manner described above, but develop preferentially within a zone of high shear strain adjacent to one of

the edges of the experimental shear zone, i.e. parallel to one of the frosted grips on the glass plates (Fig. 3e and g). During shearing from low to intermediate strains ($\gamma = 1$–3), these shear surfaces rotate synthetically, while their tips propagate at progressively decreasing angles to the SZB (Fig. 3d). Note that this propagation direction is opposite to that of shear surface tips in the experiments at atmospheric pressure. The shear surfaces then form an en-échelon pattern within the high strain zone (Fig. 3e). Compressive structures develop between the tips of adjacent, overlapping shear surfaces. These structures include elongate, dynamically recrystallized norcamphor grains and intergranular fluid pockets that together define a strong shape preferred orientation (SPO) leaning in the direction of shear (white arrows in Fig. 3f). At yet higher bulk shear strains ($\gamma = 3$–5), this SPO rotates synthetically (Fig. 3d) and fluid-filled jogs (marked 'J' in Fig. 3e and f) open at the opposite ends and sides of the adjacent, overlapping shear surfaces. The shear surfaces tend to propagate parallel to the SZB (Fig. 3d) and eventually interconnect with each other, attaining lengths of up to 1 cm. Dilation and cataclastic grain-size reduction are restricted to shear surfaces in the narrow, high-strain zone along one edge of the experimental shear zone. There, the grain size decreases with strain and attains a constant value at an even lower bulk strain ($\gamma \leq 5$) than in experiments at atmospheric pressure. The length of shear surfaces per unit area in the entire sample—including the high-strain zone—is not only lower, but also reaches a stable value at lower shear strains ($\gamma = 3.2$) than in samples deformed at atmospheric pressure.

6. Discussion

Why does confining pressure affect both the distribution and the configuration of shear surfaces, even though the average effective confining pressure ($P_e = P_c - P_f$) in experiments at both atmospheric and applied confining pressure was probably nearly zero? Any answer to this question is speculative given our current inability to control or measure pore-fluid pressure independently of confining pressure within the jacketed norcamphor samples. Certainly, the localization of deformation along fluid-filled fractures in both types of experiment indicates that effective stress gradients existed on the granular scale at the time of fracture propagation. The pore fluid pressures were probably higher in the vicinity of the shear surfaces than in the dynamically recrystallizing norcamphor matrix between the surfaces. Such effective stress gradients could not be sustained for the duration of the experiments if grain-edge fluid films were perfectly interconnected during deformation. The tendency for

the shear surfaces in the experiments at applied confining pressure to propagate at decreasing angles to the SZB with progressive shear strain suggests that both the effective stresses and the differential stress near these shear surface tips were greater than in the vicinity of extensional shear surface tips in the atmospheric pressure experiments. The latter tips are clearly dilatant and propagate at increasing angles to the SZB, indicating that the pore-fluid pressure in the vicinity of these fractures probably exceeded the atmospheric confining pressure. The difference in orientation of propagating fracture tips between the atmospheric and applied pressure experiments may therefore reflect pressure-induced differences in the local stress state within the norcamphor sample. Furthermore, they may document a pressure-induced increase in the strength of dynamically recrystallizing norcamphor.

At present, we are unable to provide a single, simple explanation for the asymmetrical, sample-scale strain pattern in the experiments at applied confining pressure. The frosted grips on the glass plates forming the SZB (Fig. 2b) are obvious sites of strain incompatibility, as observed in other rock-analogue experiments that involve simple shearing (e.g. Herwegh and Handy, 1998). Any strain-hardening of the norcamphor sample associated with increased confining pressure would accentuate such strain incompatibilities and enhance localization. Once strain localizes at the edge of the sample, the opening of fluid-filled fractures and jogs there would reduce both the local strength and the local effective stresses with respect to the rest of the dynamically recrystallizing norcamphor sample. We expect that the shear surfaces in our experiments would continue to propagate at even higher shear strains until they tap the remaining isolated fluid pockets and pore-fluid pressure gradients on the sample scale reduce to zero. Attractive as this scenario may be, however, we cannot yet rule out the possibility that the asymmetrical strain pattern in the applied pressure experiments is an artefact of the experiment itself. Experiments in which the sample strength can be measured are needed to test the working hypothesis above.

We conclude this section by noting that the pressure-dependence of rock strength is well known from triaxial deformation experiments on rocks deformed in the brittle or semi-brittle deformation regimes (review in Paterson, 1978). Unlike the strain localization patterns in our simple shear experiments, however, coaxial rock deformation under dry conditions becomes more ductile with increasing pressure ('barrelling' of coaxially flattened, cylindrical specimens, e.g. Paterson, 1978), reflecting the fact that the boundary effects in coaxial flattened samples are restricted to the vicinity of the circular platens at either end of the specimens. The simple shear experimental configuration in the

Urai–Means rig is probably closer to the kinematic boundary constraints encountered in many natural shear zones. For example, the norcamphor sample between the frosted grips defining the SZB is analogous to quartz–mica rock sheared between more competent feldspathic layers. As in our experiments, quartz–mica rock is often observed to contain synthetic shear (C') surfaces that terminate at the contacts with these layers.

7. Future applications of see-through experiments

See-through experiments at controlled pressure, temperature, and strain rate open new avenues of microstructural research that we are only beginning to explore. In addition to first observations here on the brittle to viscous transition, there are many structural phenomena that have never been directly observed during high-strain deformation. For example, syn-tectonic melting and metamorphic reactions are both pressure- and temperature-dependent processes that effect basic changes in the microstructure and rheology of deforming rocks. Mineral solubility in fluids is a pressure- and temperature-dependent property that governs dissolution-precipitation in rocks and is potentially the rate-controlling process in several deformation mechanisms, including diffusion-accommodated grain-boundary sliding (Paterson, 1995) and fracture-healing during episodic frictional sliding on fault surfaces (Blanpied et al., 1995). Characterizing such deformational processes by analysing microstructures is the first step towards refining existing flow laws and developing new constitutive equations. Such equations are essential for predicting the rheology of geological materials at natural conditions and over long time periods. Deforming rock analogues under changing pressures, temperatures and/or strain rates is useful for investigating the rates of microstructural change associated with different deformation mechanisms during burial or exhumation. Such studies may yet provide geologists with reliable criteria for determining what part of a rock's P–T–t history is preserved in its microstructure. Finally, further development of the experimental system presented above, including provisions for conducting drained experiments at controlled pore fluid pressure, will enable more sophisticated investigation of fluid migration mechanisms in fault rocks.

Acknowledgements

References

Blanpied, M.L., Lockner, D.A., Byerlee, J.D., 1995. Frictional slip of granite at hydrothermal conditions. Journal of Geophysical Research 100, 13045–13064.

Bons, P.D., 1993. Experimental deformation of polyphase rock analogues. Geologica Ultrajectina 110, 1–207.

Bons, P.D., Jessell, M.W., Passchier, C.W., 1993. The analysis of progressive deformation in rock analogues. Journal of Structural Geology 15, 403–411.

Herwegh, M., Handy, M.R., 1996. The evolution of high temperature mylonitic microfabrics: evidence from simple shearing of a quartz analogue (norcamphor). Journal of Structural Geology 18, 689–710.

Herwegh, M., Handy, M.R., 1998. The origin of shape preferred orientations in mylonite: inferences from in-situ experiments on polycrystalline norcamphor. Journal of Structural Geology 20, 681–694.

Herwegh, M., Handy, M.R., Heilbronner-Panozzo, R., 1997. Temperature and strain rate dependent microfabric evolution in monomineralic mylonite: Evidence from in-situ deformation of a rock analogue. Tectonophysics 280, 83–106.

Holness, M.B., 1997. The permeability of non-deforming rock. In: Holness, M.B. (Ed.), Deformation-enhanced Fluid Transport in the Earth's Crust and Mantle, The Mineralogical Society Series 8, pp. 9–34.

Means, W.D., 1977. A deformation experiment in transmitted light. Earth and Planetary Science Letters 35, 169–179.

Means, W.D., 1980. High temperature simple shearing—An experimental approach. Journal of Structural Geology 2, 197–202.

Means, W.D., 1981. The concept of steady state foliation. Tectonophysics 78, 178–199.

Means, W.D., 1989. Synkinematic microscopy of transparent polycrystals. Journal of Structural Geology 11, 163–174.

Means, W.D., Xia, Z.G., 1981. Deformation of crystalline materials in thin section. Geology 9, 538–543.

Mosher, S., Berger, R.L., Anderson, D.E., 1975. Fracturing characteristics of two granites. Rock Mechanics 7, 167–176.

Paterson, M.S., 1978. Experimental rock deformation—the brittle field. Springer-Verlag, Berlin.

Paterson, M.S., 1995. A theory for granular flow accommodated by material transfer via an intergranular fluid. Tectonophysics 245, 135–151.

Platt, J.P., Vissers, R.L.M., 1980. Extensional structures in anisotropic rocks. Journal of Structural Geology 2, 397–410.

Tullis, T.E., Tullis, J., 1986. Experimental rock deformation techniques. In: Hobbs, B.E., Heard, H.C. (Eds.), Mineral and Rock Deformation: Laboratory Studies. The Paterson Volume,

Geophysical Monograph 36. American Geophysical Union, pp. 297–324.

Urai, J.L., 1983. Deformation of Wet Salt Rocks. Ph.D. thesis, University of Utrecht.

Vauchez, A., 1987. The development of discrete shear zones in a granite: stress, strain, and changes in deformation mechanisms. Tectonophysics 133, 137–157.

Weijermars, R., 1986. Flow behaviour and physical chemistry of bouncing putties and related polymers in view of tectonic laboratory applications. Tectonophysics 124, 325–358.